

Supplementary material for Deep learning for denoising High-Rate Global Navigation Satellite System data

A. M. Thomas^{1,*}, D. Melgar¹, S. N. Dybing¹, and J. R. Searcy²

¹Department of Earth Sciences, University of Oregon, Eugene, Oregon, USA

5 ²Data Science Initiative, University of Oregon, Eugene, Oregon, USA

*Corresponding author: a.firstauthor@university.edu

Author ORCIDiDs

A. M. Thomas: 0000-0001-6997-3140

D. Melgar: 0000-0001-6259-1852

10 S. N. Dybing: 0000-0002-9274-6568

J. R. Searcy: 0000-0003-3544-3066

Supplemental Material

15 Figures showing the architectures of Model 1 (v1_plot.h5.svg), Model 2 (v2_plot.h5.svg), and Model 3 (v3_plot.h5.svg) are available in the Github and Zenodo repositories that accompany the manuscript.

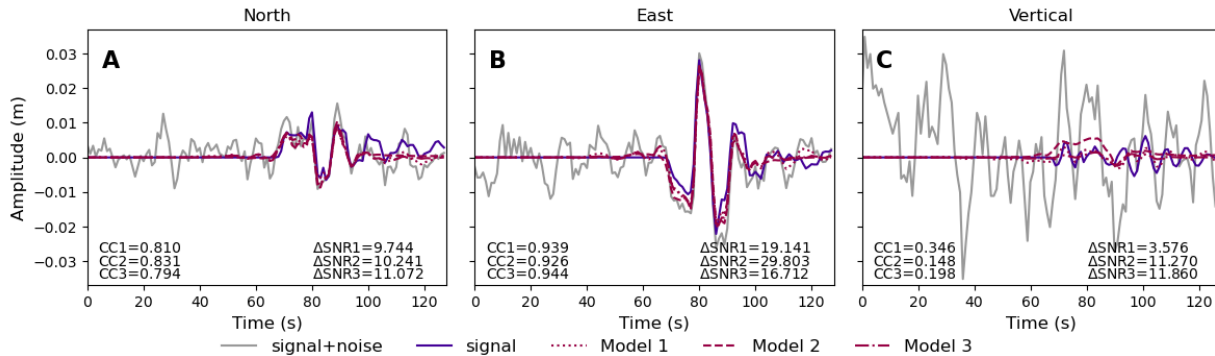
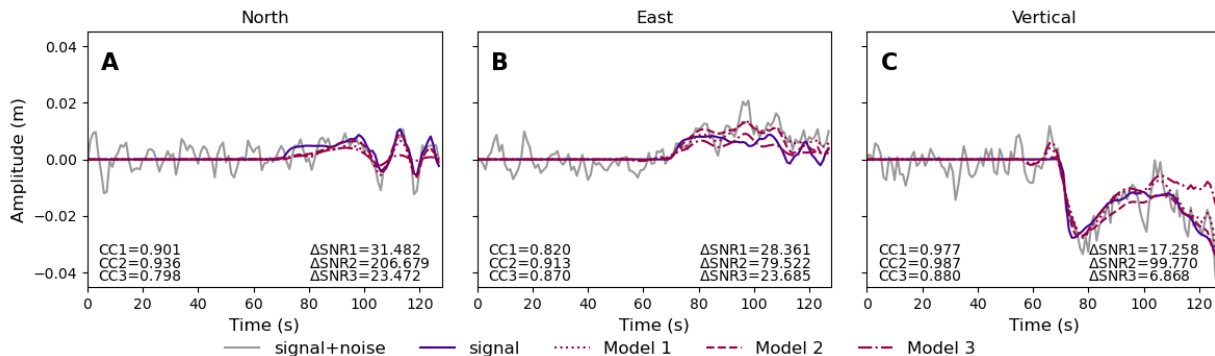


Figure S1. Performance of Models 1, 2, and 3 on a common example.



20

Figure S2. Performance of Models 1, 2, and 3 on a common example.

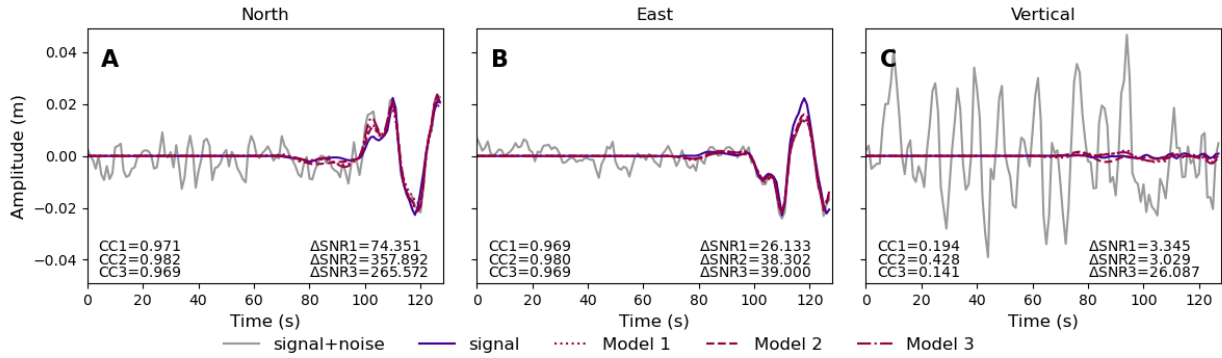
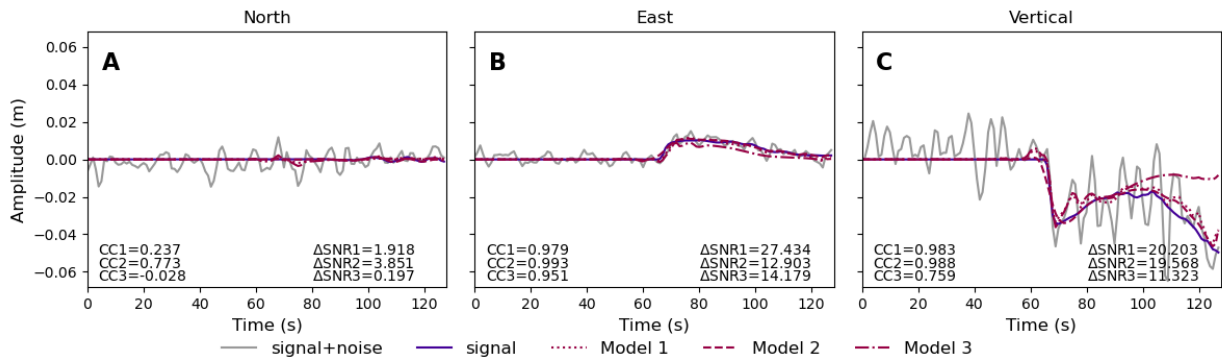


Figure S3. Performance of Models 1, 2, and 3 on a common example.



25 Figure S4. Performance of Models 1, 2, and 3 on a common example.

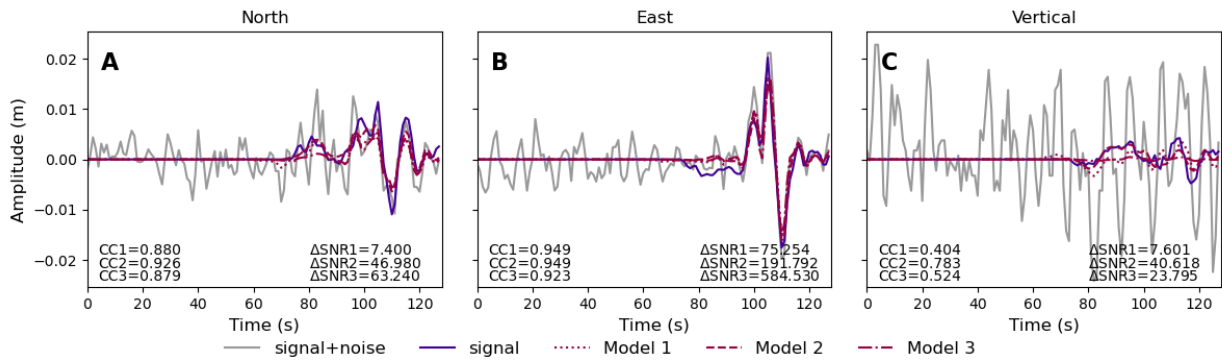


Figure S5. Performance of Models 1, 2, and 3 on a common example.

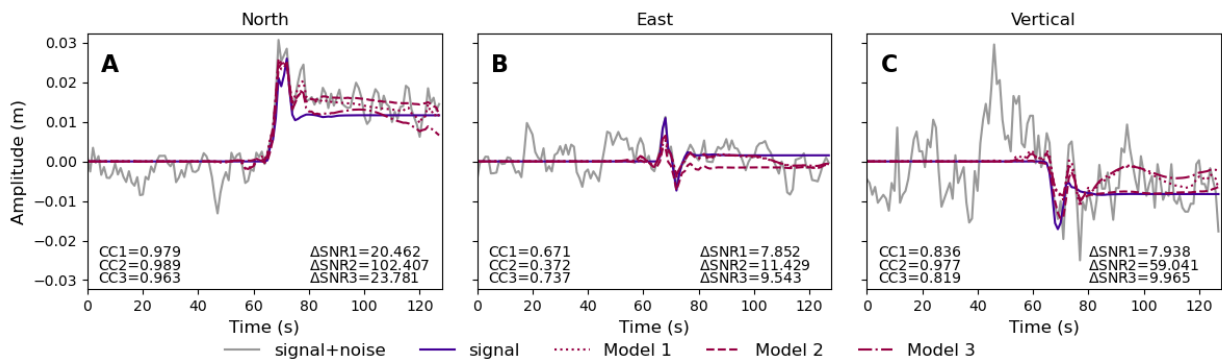


Figure S6. Performance of Models 1, 2, and 3 on a common example.

30

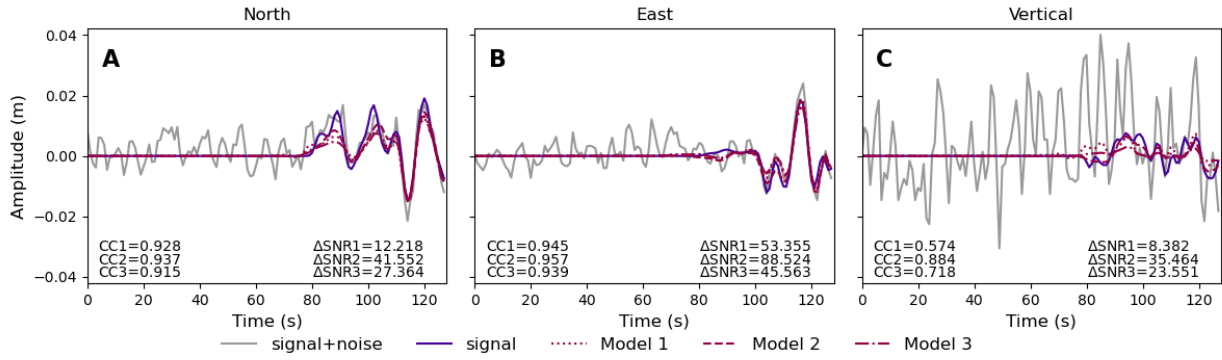


Figure S7. Performance of Models 1, 2, and 3 on a common example.

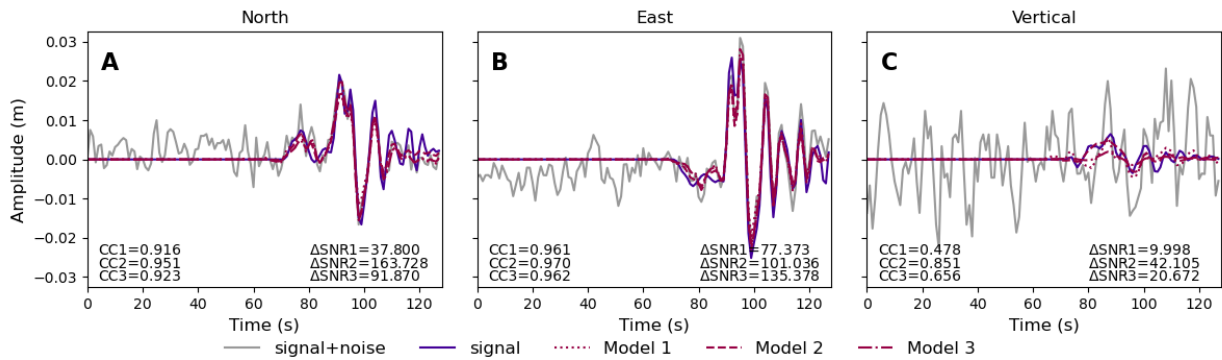
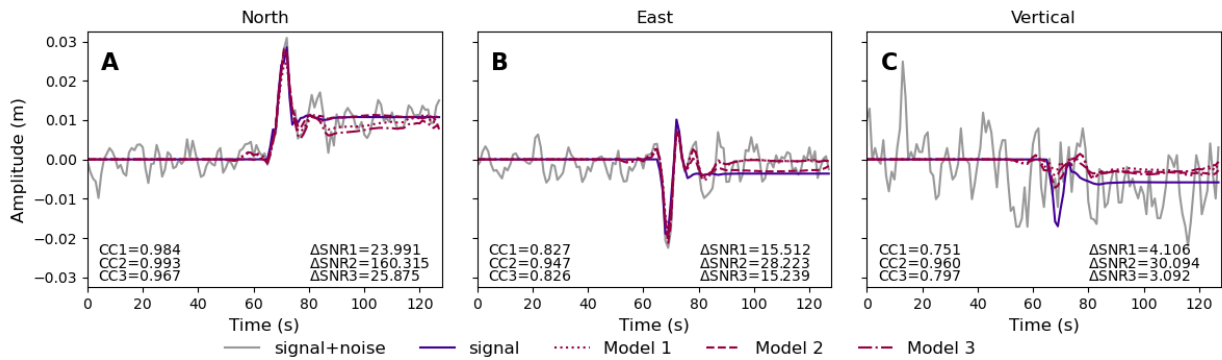


Figure S8. Performance of Models 1, 2, and 3 on a common example.



35 Figure S9. Performance of Models 1, 2, and 3 on a common example.

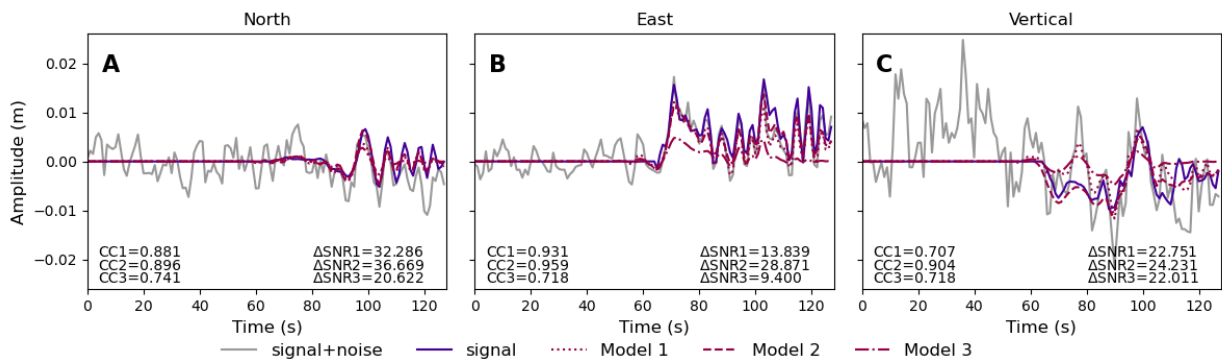


Figure S10. Performance of Models 1, 2, and 3 on a common example.

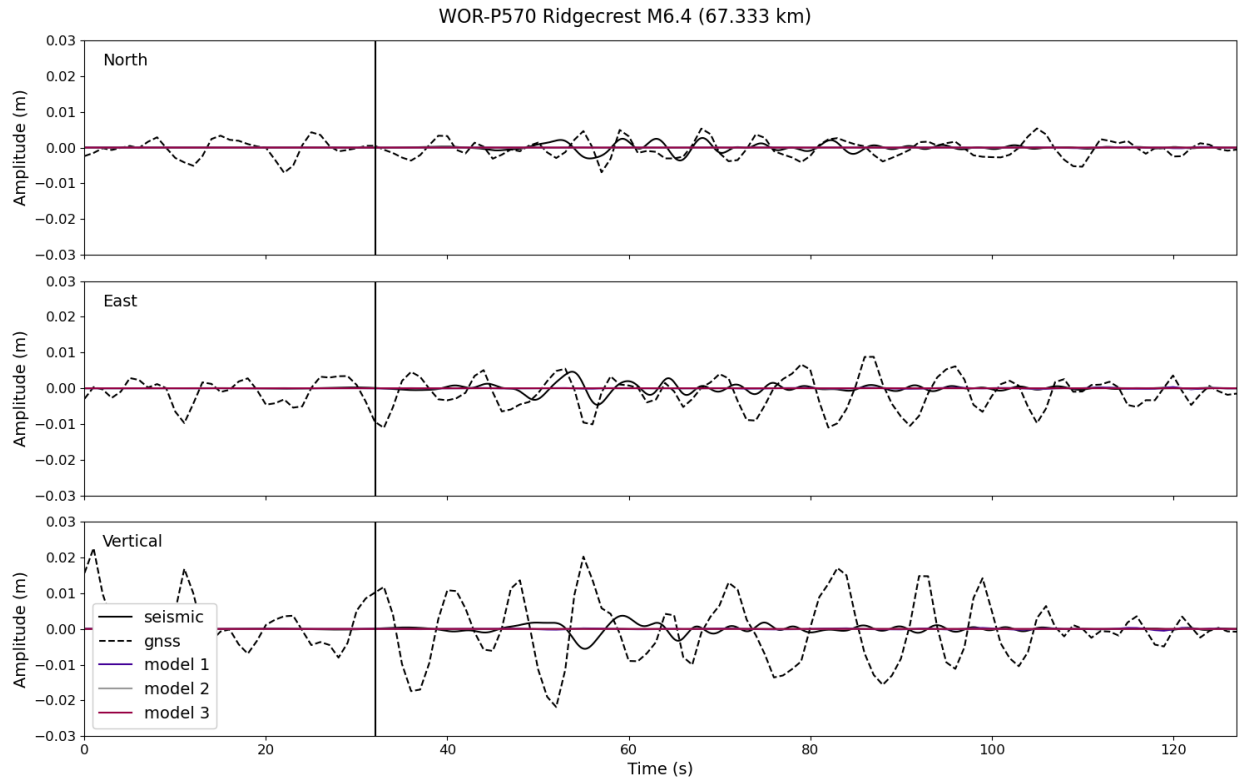
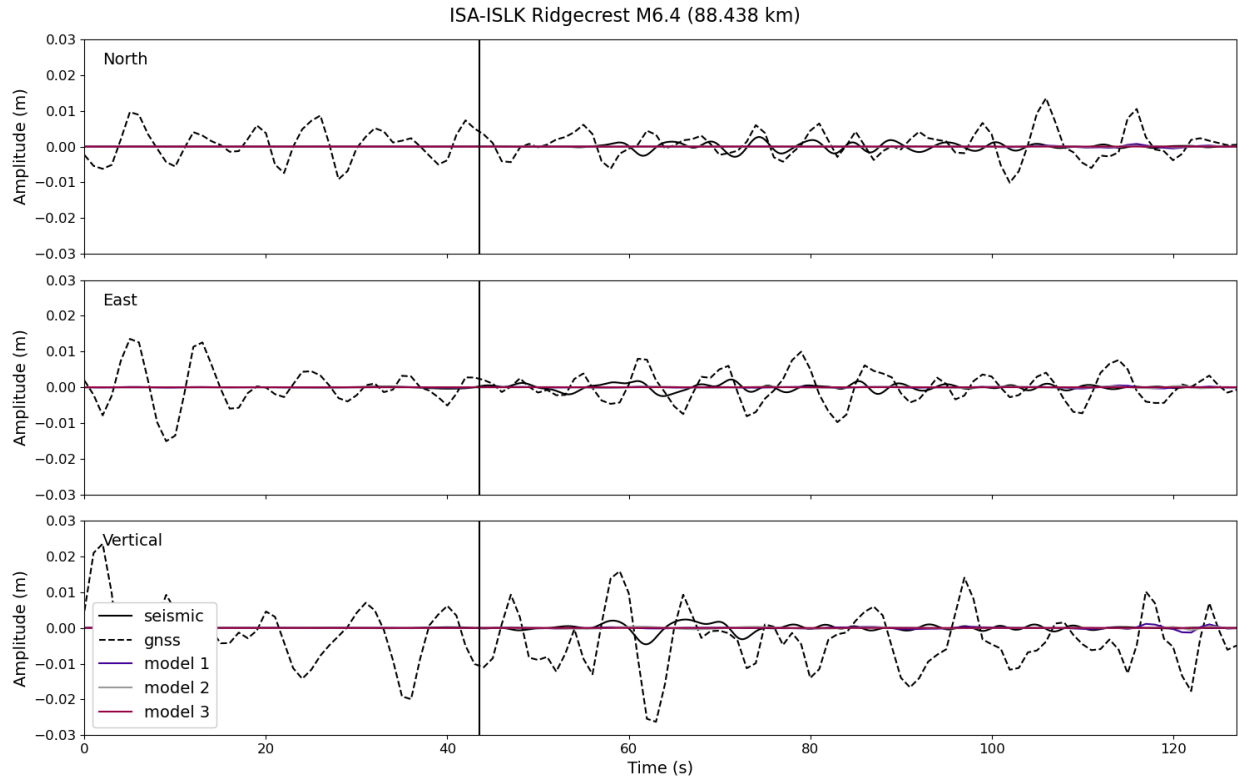
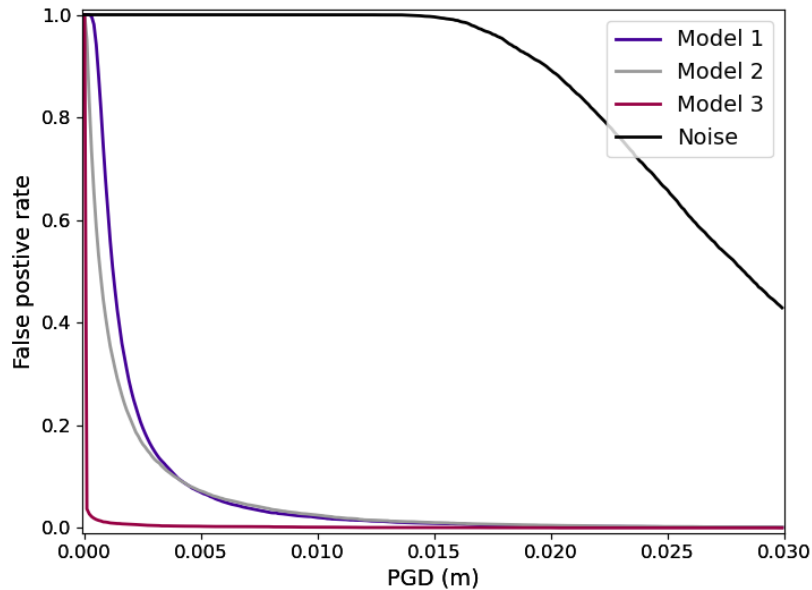


Figure S11. Comparison of recordings of the M6.4 Ridgecrest earthquake at strong motion station WOR and GNSS station P570. GNSS and integrated strong motion data are shown as dashed and solid black lines respectively. GNSS records denoised by models 1, 2, and 3 are shown in blue, grey, and pink respectively. Vertical black line shows the theoretical P-wave arrival time.



50 *Figure S12. Comparison of recordings of the M6.4 Ridgecrest earthquake at strong motion station ISA and GNSS station ISLK. GNSS and integrated strong motion data are shown as dashed and solid black lines respectively. GNSS records denoised by models 1, 2, and 3 are shown in blue, grey, and pink respectively. Vertical black line shows the theoretical P-wave arrival time.*



55

Figure S13. The false positive rate of Models 1, 2, and 3 applied to unseen noise data ($N=10000$) plotted against a PGD decision threshold. For comparison we also show the PGD of the noise waveforms the models are applied to. The false positive rate at a decision threshold of 1 cm PGD is 2.05%, 2.51%, and 0.16% for Models 1, 2, and 3 respectively. The false positive rate at a decision threshold of 21 cm PGD is 0.4%, 0.53%, and 0.06% for Models 1, 2, and 3 respectively.

60